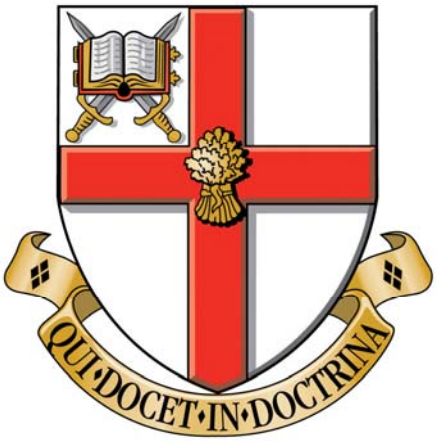

University of Chester

Author(s): R J Price ; D Blazina ; G C Smith ; T J Davies

Title**:** Understanding the impact of cavitation on hydrocarbons in the middle distillate range

Date: 2015. Available online 22 April 2015

Originally published in: Fuel

Example citation: Price, R. J., Blazina, D., Smit, G. C., Davies, T. J. (2015). Understanding the impact of cavitation on hydrocarbons in the middle distillate range. *Fuel, 156*, 30-39

Version of item: Author's post-print

Available at: http://hdl.handle.net/10034/553066

Understanding the Impact of Cavitation on Hydrocarbons in the Middle Distillate Range

R. J. Price[a,*], D. Blazina[a], G.C. Smith[b], T. J. Davies[b]

[a]Shell Global Solutions, Concord Business Park, Threapwood Road, Manchester, M22 0RR, United Kingdom

[b]Natural Sciences, University of Chester, Thornton Science Park, Pool Lane, Ince, Chester, CH2 4NU, United Kingdom

Abstract

Hydrocarbons in the middle distillate range (C_8–C_{26}) have been treated with ultrasound at 20 kHz – a frequency sufficient to drive acoustic cavitation. The high temperatures experienced as a result of the implosion of fuel vapour bubbles are sufficient to produce pyrolytic degradation and dehydrogenation, as well as a growth mechanism that results in the formation of small particles that have similarities with the primary soot particles produced during diesel combustion. These nanosized particles agglomerate as a result of kinetically driven collisions during cavitation to form a dispersion of micron sized particles in the treated hydrocarbon. The particles are carbonaceous in character, being a mixture of amorphous and graphitic-like carbon. The mass of material produced increases with the C/H atomic ratio of the hydrocarbon undergoing cavitation and is decreased through the addition (1–3 %v/v) of low boiling paraffinic hydrocarbons, possibly as a result of lowering the temperature developed inside imploding cavities. Dispersions of microparticles contain equilibrated levels of nanoparticles. If sufficiently high numbers of these smaller primary particles are present they agglomerate due to thermally driven collisions during post-cavitation storage. When this happened a sharp rise in the number of 1–2 µm particles was seen after only a few

days. Some evidence is presented for the behaviour of ultrasonically treated hydrocarbons being related to the degradation of diesel fuel exposed to hydrodynamic cavitation in the fuel systems of modern common rail direct injection diesel engines.

Keywords: Cavaitation, microparticles, middle distillate hydrocarbons, nanoparticles, pyrolytic degradation, ultrasound.

*Corresponding author: Tel:. + 44 161 49 94 515

Email address: richard.price@shell.com

1. Introduction

Ultrasound has become a common laboratory tool used to generate acoustically driven cavitation and chemical reactions in liquids (sonochemistry) [1,2]. The compression and rarefaction of the sound waves when passed through a liquid produces bubbles; the formation, growth and collapse of which is known as cavitation. These bubbles, which are comprised of vapour and dissolved gases, shrink and expand under the influence of the acoustic field. Individual bubbles experience interference from their surroundings and consequently expansion to an unstable size can result, followed by an implosive collapse. This produces localised hot spots (~5,000 K) which are characterised by very rapid heating and cooling rates (>10^9 K s^{-1}) [3–7].

The acoustic sonication of a range of hydrocarbons that fall within the middle distillate range (C_8–C_{26}) has now been studied as a means of simulating some of the chemistry that may occur in diesel fuel whilst in the high pressure fuel systems of modern common rail direct injection compression ignition engines. The cavitation of fuel in these systems is hydrodynamic in origin, as opposed to acoustic, and can result from the pressure drop across an orifice or when fast moving flows turn sharp corners. Some of the first reports of non-aqueous sonochemistry were published over fifty years ago and suggest that the sonication of aromatic and heterocyclic compounds produces ring cleavage and acetylene production [8–10]. Subsequently Suslick and co-workers found that alkanes undergo sonochemical reactions which are similar to high temperature (>1,200 °C) pyrolysis [11]. For example, the products of *n*-decane sonolysis are hydrogen, methane, acetylene and a series of alkenes including ethylene, propylene, butene, pentene, etc. This is consistent with the operation of a radical chain Rice mechanism [12]. Riesz and Misik in related work trapped and identified the radicals produced during the sonolysis of a number of different organic liquids, including *n*-alkanes. Their results were also consistent with a pyrolysis mechanism [13,14].

Cataldo found that the prolonged sonication of benzene, toluene, styrene and tetralin produced insoluble dark matter [15]. Infrared spectroscopy of the material from benzene sonolysis suggested that the product contained a cross-linked structure similar to radiation-damaged polystyrene. Decalin and tetralin sonication caused aromatization reactions, although decalin was also cracked to *o*-xylene and ethylene. Somewhat similar findings have also been reported by Katoh and co-workers, who produced C_{60} fullerene from benzene sonolysis [16]. In subsequent work, the same group produced carbon nanotubes by applying ultrasound to liquid chlorobenzene containing suspended $ZnCl_2$ particles [17]. A large number of sono-polymerisation reactions have also been reported [18–22].

Four different types of reaction have therefore been observed in the ultrasonic destruction of non-aqueous liquids: Radical pyrolysis, thermal cracking, radical polymerisation and dehydrogenation. This results in the possibility of both larger and smaller molecules being formed in hydrocarbons that have undergone cavitation.

In 1995 Price and co-workers explored the possibility of using ultrasound for accelerated aging of diesel fuels in an attempt to predict long-term storage stability [23,24]. Common rail high pressure diesel injection systems were not widely available in the market at this time. Experiments with dodecane showed evidence for thermal cracking after 20 hours of sonication, with detection of C_7–C_{10} species by gas chromatography mass spectrometry. After automotive grade diesel was sonicated for >6 hours, sediment was produced with an average molecular weight of 40,000 amu. The material was deep brown in colour, almost completely soluble in terahydrofuran (THF) and had a UV-Vis absorption spectrum characteristic of aromatic species. Infrared analysis suggested the presence of ester carbonyl groups, unsaturated hydrocarbons and possibly indole-like groups.

More recently an experimental investigation into the impact of hydrodynamic cavitation on diesel has been reported by Lockett and Jeshani [25]. Samples of commercial diesel were

subjected to 40 hours of cavitation across an injector at a pressure of 550 bar. The fuel was cooled to 70 °C after cavitation before being re-cycled through the injector. The optical absorptivity of each diesel at 405 nm was observed to increase as a result of chemistry undergone by aromatic hydrocarbons present in the fuels. The increase in absorptivity was found to be greater for fuel exposed to both cavitation and temperature than for fuel maintained at 70 °C for 40 hours in a water bath. Additionally it was found that a greater increase in absorptivity during cavitation was observed for fuel that had been stored for a year before testing.

This paper reports the results of ultrasound experiments on a number of pure hydrocarbons (1-methylnaphthalene, decalin, tetralin, hexadecane) and hydrocarbon mixtures (diesel and 1-methylnaphthalene combined with a range of different aromatic, naphthenic and paraffinic hydrocarbons to make two component mixtures). The formation of insoluble products generated by cavitation has been studied along with the critical physical and compositional properties of the liquids that control the chemistry taking place. This is related to the behaviour of diesel fuel in the high pressure fuel systems of common rail direct injection compression ignition engines.

2. Experimental

2.1 Ultrasound treatment of hydrocarbons

Sonication experiments were carried out with a VCX 500 ultrasonic processor (ex. Sonics Materials Inc.) and a 13 mm extender horn which delivers ultrasound to a 50 mL sample of hydrocarbon contained within a jacketed glass beaker. Cold water (5 °C) was passed through the jacket to keep the liquid hydrocarbon below its flash point – for safety reasons a cut-off temperature was set at 55 °C. A PTFE lid was used to prevent splashing whilst dry air was blown over the surface of the fuel to ensure that there was no condensation

inside the reaction vessel (Fig. 1). The whole apparatus was housed inside a box fitted with a safety cut-out mechanism and insulated to reduce acoustic noise.

{Fig.1 here}

Ultrasound is produced at a frequency of 20 kHz and when the amplitude of the processor is set to 65% the transfer of energy to the hydrocarbon occurs at 6 kJ mL^{-1} h^{-1}. The probe is made of titanium alloy (Ti 6Al-4V) and consists of 90% titanium, 6% aluminium and 4% vanadium. This material is susceptible to cavitation erosion and becomes tarnished during use. The probe was polished on silicon carbide paper between each experiment to maintain a smooth and shiny tip surface.

In a typical experiment 50 mL of hydrocarbon was sonicated for a set period of time, during which a darkening occurred due to the build-up of a dispersion of carbonaceous particles. Gravimetric analysis of these particles was carried out by adding 50 mL of *n*-heptane to the sonicated hydrocarbon and shaking. The sample was then split between two centrifuge tubes and spun at 4,000 r min^{-1} for 20 minutes. The deposit sediment was collected, dried and weighed on a 0.7 µm Whatman glass microfiber filter (Grade GF/F).

2.2 Hydrocarbon materials

Hydrocarbons were sourced from the Sigma-Aldrich Corporation in their highest available purity. The diesel fuel used was an EN590 'zero' sulphur diesel (sulphur <10 ppm, density 0.844 g cm^{-3}, viscosity 2.8 mm^2 s^{-1} at 40 °C , water content 45 mg/kg, mono-aromatics 27.1 %m/m, di-aromatics 3.5% m/m, tri-aromatics 0.4%m/m, carbon 86.4 %m/m, hydrogen 13.1% m/m, oxygen <0.04 %m/m) which contained no performance additives or fatty acid methyl ester (FAME). Before treatment with ultrasound all samples were filtered through a 0.7 µm Whatman glass microfiber filter (Grade GF/F).

2.3 Laser particle counting

Particle analysis was carried out using a Spectrex LPC-2200 laser particle counter (Spectrex Corporation, Redwood City, CA.) which makes measurements based on the principle of near-angle light scattering. A revolving laser beam is passed through the walls of a glass container; any particles present in the fuel sample cause the beam to scatter. The extent of scattering is proportional to the number and size of the particles, which are reliably counted in the 1 to 100 µm size range. Samples were agitated on a mechanical shaker (300 r min^{-1}, 1 minute) before standing to allow any air bubbles to settle. Particle counts were then based on the average of three consecutive measurements.

When the number concentration is higher than 1,000 cm^{-3} there is a risk of overlap between particles in the third dimension (i.e. closer to or further from the detector) which may lead to two or more small particles being counted as a single large particle. Sample dilution with chromatography grade *n*-heptane, which has a very low background particle count (< 20 cm^{-3}), prevents this artefact from occurring.

2.4 Transmission Electron Microscopy (TEM)

Samples were prepared for TEM analysis by mechanically agitating the sonicated liquids for 1 hour before taking a 3 mL aliquot and diluting with 15 mL of *n*-heptane. The resulting suspension was then filtered onto a holey carbon film 300 mesh copper TEM grid and de-oiled using a capillary heptane wash. Imaging was carried out in transmission mode using a JEOL 2100 TEM (JEOL Ltd, Tokyo) at 200 kV beam voltage. TEM-EDX analyses were made using an Oxford Instruments INCA system with an X-max-80 silicon drift detector (Oxford Instruments Ltd, Oxford, UK).

2.5 X-ray Diffraction (XRD) and SEM-EDX

Samples were prepared for XRD by filtration from the sonicated liquids onto 0.4 μm track-etched membrane filters (Whatman Nuclepore-type) from which the solids were transferred onto low-diffraction silicon substrates. XRD measurements were made using Ni-filtered Cu Kα radiation in a PANalytical X'pert Pro diffractometer (PANalytical B.V., Almelo, The Netherlands). In some cases, SEM-EDX measurements were made of the approximate composition of the samples prepared for XRD, while still in place on the XRD substrate, using a Zeiss EVO60-XVP SEM (Carl Zeiss Ltd, Cambridge, UK) equipped with an Oxford Instruments INCA system with an X-max-80 silicon drift detector (Oxford Instruments Ltd, Oxford, UK).

2.6 X-ray Photoelectron Spectroscopy

XPS was carried out using a purpose-built ultra-high vacuum system equipped with a Specs PHOIBOS 150 electron energy analyser and Specs FOCUS 500 monochromated Al Kα X-ray source (Specs GmbH, Berlin, Germany). As for XRD, samples were prepared for analysis by filtration and subsequent drying from heptane slurry onto clean gold foil substrates.

3. Results

Ultrasound treatment (1 h) of liquid hydrocarbons in the middle distillate boiling range produced a variety of visual changes. Hexadecane (b.p. 287 °C) and decalin (b.p. 189°C) changed from colourless to pale yellow. The yellow diesel fuel (b.p. 162–362 °C) darkened in colour, whereas the pale yellow 1-methylnaphthalene (b.p. 240 °C) turned black as a result of the formation of a suspension of fine particles (Fig. 2). The particulate matter dispersed in the 1-methylnaphthalene was removed by centrifuge and filtration, allowing the mass of material to be determined.

{Fig. 2 here}

The morphology of the particles formed by ultrasound cavitation is presented in the three TEM images in Fig. 3. The lowest magnification (Fig. 3a) shows that the sample consists of irregular shaped material of varying contrast ranging from 500 nm to 5 μm in size. Images at higher magnification reveal the presence of smaller primary nanoparticles (Fig. 3b). There is also evidence that these primary particles can overlap and agglomerate, and that they have an internal morphology (Fig. 3c). This is reminiscent of the graphitic planes that are observed in diesel combustion soot or carbon black. TEM-EDX was used to determine the elemental composition of the material. Copper, present in the support grid and sample holder was ignored to give the elemental composition of the material shown in Fig. 3a as carbon 96.4, oxygen 3.5 and sulphur 0.1 atomic %. Significant proportions of the carbon detected will have arisen from the carbon grid upon which the particles were captured. Hydrogen is not detected by this technique and is therefore excluded from the atomic % values given here and subsequently in this work.

XRD was carried out on a larger sample prepared by sonicating 1-methylnaphthalene for 2 hours followed by centrifuge and filtration onto a track-etched membrane filter. The diffraction pattern shows a broad background feature between 10° and 30° with a peak at approximately 23° – this is positioned at a lower angle (larger interplanar spacing) than expected for pure graphite (26.4°) and is indicative of disordered graphitic-like carbon (Fig. 3d). From the other peaks in the spectrum it is possible to make an unambiguous identification of titanium crystals, which are present as a consequence of cavity induced erosion of the ultrasound probe tip. Analysis by SEM-EDX after accounting for the substrate, confirmed the carbonaceous character of the material with an elemental composition of carbon 88.0, oxygen 9.9, titanium 1.1, fluorine 0.3, sulphur 0.3 and nickel 0.2 atomic %, with traces of copper, vanadium, calcium and iron.

{Fig. 3 here}

XPS analysis of further samples prepared in the same way gave elemental composition consistent with the SEM-EDX analysis and also showed a low level of nitrogen (carbon 88.0, oxygen 11.0 nitrogen 0.6 and sulphur 0.4 atomic %). In a similar fashion to TEM-EDX and SEM-EDX, hydrogen is not detected by this technique and the results are therefore given excluding this element. The carbon 1s photoelectron spectrum comprised of a main peak (285.0 eV) with slight asymmetry on the high binding energy side (Fig. 4a). An X-ray excited carbon KVV Auger spectrum was also collected and the shape and kinetic energy of the high energy onset were consistent with a proportion of graphitic-like material being present (Fig. 4b) [26]. Highly ordered graphite would be expected to show a prominent π–π^* shake-up feature at 291.7 eV in the XPS – this was not present suggesting that the graphite-like material in the sample may only have short-range order. Curve-fitting on the high energy side of the main carbon 1s peak is consistent with carbon-oxygen bonding and in samples generated from diesel fuel was attributed more specifically to C–O (286.5 eV), C=O (287.8 eV) and C(O)O (289.3 eV) ester or acid groups. Likewise the oxygen 1s photoelectron peak was fitted with two components representing single and double bonds to carbon.

{Fig. 4 here}

Ultrasound experiments in which the probe was not placed directly into the hydrocarbon being treated were also conducted in order to avoid titanium contamination of the samples and to make sure that the production of particles was not due to the metal acting as a dehydrogenation catalyst. A cup-horn was used to transfer ultrasound through the walls of a small conical flask filled with 25 mL of hydrocarbon – an arrangement somewhat akin to that of a high intensity ultrasonic bath. The efficiency with which energy was transferred was approximately a factor of ten lower than when placing a sonication probe directly into the hydrocarbon. 1-Methylnaphthalene was treated by this method for 5 hours, over which time

a black suspension of particles was formed. TEM imaging (Fig. 5) showed the morphology of the material to be similar to that generated in earlier experiments. The elemental composition determined by TEM-EDX was also the same, although in this instance no titanium was present. A further sample was produced in which the treatment of 1-methylnaphthalene with ultrasound was carried out under a nitrogen atmosphere. The hydrocarbon was not fully degassed and therefore still contained small levels of dissolved air. The formation of black particles again took place.

{Fig. 5 here}

The relationship between deposit mass and length of sonication time was found to be linear for 1-methylnapthalene (Fig. 6). However, the varying degree of colour change observed between different fuels suggests that the deposit-forming tendency is also dependent on the degree of unsaturation in the molecular structure of the hydrocarbon being treated. Fig. 7 presents the gravimetric analysis after 1 hour ultrasound treatments of four different fuels: 1-methylnaphthalene and mixtures of 80% v/v 1-methylnapthalene with 20% v/v of tetralin, decalin and hexadecane. Deposit formation appears to be linearly dependent on C/H atomic ratio. EN590 market diesel typically has a C/H of 0.50–0.55 but is comprised of different generic classes of hydrocarbons, the atomic ratios of which are presented as horizontal grey bars marked below the x-axis in Fig. 7.

{Fig. 6 and 7}

Samples of 1-methylnaphthalene were prepared with 1, 2 and 3% v/v of *n*-octane, *n*-decane, dodecane, tetradecane, hexadecane, ethylbenzene, *n*-propylbenzene, indan and indene. The fuels were treated with ultrasound for 1 hour in a randomised order which included ten repeat tests on 1-methylnapthalene to establish a baseline level of deposit formation and an indication of the repeatability of the test method. The relative standard deviation of the deposit mass from 1-methylnapthalene was 2.8% (n=10).

The change in deposit mass resulting from the incorporation of different hydrocarbons was found to be minimal for the aromatic hydrocarbons (indan, indene, *n*-propylbenzene and ethylbenzene) (Fig. 8). In contrast the presence of paraffinic hydrocarbons reduced the amount of deposit, with this trend becoming more pronounced as the alkane chain length became shorter. Generally, but not always, the suppression of deposit formation increased with the blend ratio of the alkane.

{Fig. 8 here}

A 'zero' sulphur diesel fuel which contained no performance additives or FAME was treated with ultrasound for different periods of time, up to 80 minutes. This was followed by a determination of the 1–100 μm particle count in each sample. 1-Methylnaphthalene was sonicated for 5 minutes before carrying out a similar analysis. Fig. 9 shows a monotonically increasing particle count in the diesel fuel as the exposure to ultrasound was increased. The particle count in the 1-methylnaphthalene sample treated for 5 minutes was 30% higher than the equivalent diesel sample; however the variation of number concentration with particle size for these two samples was quite different (Fig. 10). The majority of the particles (>98%) were <16 μm in size but the mean particle diameter ($d_{1,0}$) in diesel fuel was smaller (2.1–2.7 μm) than in 1-methylnphthalene (6.6 μm). This indicates a higher particle mass concentration for 1-methylnaphthalene, consistent with the previously established high deposit-forming tendency of the di-aromatic when exposed to cavitation.

{Fig. 9 and 10}

All the samples were allowed to stand under ambient conditions in the laboratory and periodically the particle count measurements were repeated over 33 days. Diesel fuel that has not undergone cavitation has a low particle count of <1,000 cm^{-3} which does not significantly change with storage time (Fig. 11 and Table 1). The initial particle count for the 5 minute sample was higher (7,000 cm^{-3}) but again did not change. The diesel sample treated for 20

minutes underwent a small increase in particle count after 1 day, the count then became stable. This initial increase in particle count for the diesel sample exposed to ultrasound for 80 minutes was more pronounced, but again stabilised after 1 day. The sonicated 1-methylnaphthalene sample showed distinctive behaviour in that the particle count increased fourfold after 1 day. This rapid increase continued and after 7 days storage the particle count had increased by a factor of 14; beyond this storage time the rate of increases slowed and the count eventually stabilised. This increase in number concentration was combined with a drop in the mean diameter of the particles present from 7 μm to 2 μm.

{Fig. 11 and Table 1 here}

4. Discussion

4.1 The impact of hydrocarbon composition and physical properties on deposit formation

Two key parameters associated with fluid cavitation are the number of bubbles generated and the intensity of the bubble collapse (which is related to the speed of collapse and the magnitude of the temperature and pressure generated). The critical parameters that have a controlling influence are:

Ambient pressure: Increasing the external pressure raises the threshold of cavitation as larger negative pressures are required to separate molecules to form a bubble.

Fuel vapour pressure: When bubbles form they contain fuel vapour and any dissolved gases that are present. High vapour pressures actually soften the collapse of bubbles and reduce the harshness of the conditions that develop, i.e. lower peak temperature and pressure.

Viscosity: Liquids with higher viscosity have stronger cohesive forces and are consequently harder mediums in which to induce cavitation.

Surface tension: Decreasing surface tension makes the formation of cavities more likely to occur, however the relationship is complex and not well understood.

Temperature: Increasing temperature decreases surface tension and viscosity and increases vapour pressure. All three changes make cavitation more likely.

Dissolved gasses and suspended particles: These can act as nuclei for bubble formation.

The maximum pressure and temperature that occur inside a collapsing bubble have been defined by assuming adiabatic conditions [27,28]:

$$p_{max} = p\,(p_c\,(\gamma - 1)/p)^{\gamma/(\gamma-1)} \quad (1)$$

$$T_{max} = T_0\,(p_c\,(\gamma - 1)/p) \quad (2)$$

where T_0 is the ambient temperature (K) of the liquid, γ is the ratio of heat capacity of the bubble gas at constant pressure (C_p) and volume (C_V), p is the pressure (N m^{-2}) in the bubble at its maximum size (assumed to be the vapour pressure of the liquid) and p_c is the pressure (N m^{-2}) in the liquid at the moment of collapse (which is the sum of the ambient liquid pressure and the ultrasound amplitude during sonication).

The conditions generated during collapse are extreme, however an important observation from sonochemistry studies is that as the temperature of the fluid being cavitated is raised the vapour pressure (p) inside the bubble increases and consequently T_{max} decreases (equation 2). Therefore, the reaction rates of the chemistry taking place within a collapsing bubble are counter intuitively slowed by raising the temperature (T_0) and increasing the vapour pressure (p) of the liquid. This has been clearly demonstrated by Suslick and co-workers who measured depletion of 2,2-diphenyl-1-picrylhydrazyl (DPPH) used to trap the radicals formed by cavitation collapse in a number of organic liquids exposed to ultrasound [29]. The rate of depletion of DPPH is proportional to the rate of radical production by cavitation and was found to be inversely related to the vapour pressure of hydrocarbon being treated.

From the data present in Fig. 7 and 8 it is apparent that the rate of cavity induced deposit formation is related to both the degree of unsaturation (C/H ratio) and the vapour pressure of the hydrocarbon undergoing sonication. The fuels from Fig. 8 all underwent standard analysis to define three properties: flash point (related to the vapour pressure of the fuel), kinematic viscosity at 40 °C and C/H atomic ratio. In an empirical treatment of the data, deposit mass determined by gravimetric analysis was correlated against fuel compositions and properties. Carbon-to-hydrogen atomic ratio is the single most influential fuel property with respect to deposit formation, followed by flash point and lastly viscosity. However, the best regression of the data ($R^2 = 0.73$) is achieved when using all three properties (Fig. 12)

$$Deposit\ mass = (28.05 * C/H) + (0.02 * f_p) - (2.77 * V_k) - 22.15 \quad (3)$$

where f_p is flash point (°C), V_k is the kinematic viscosity (mm^2s^{-1}) at 40 °C and *C/H* is the atomic carbon-to-hydrogen ratio.

{Fig. 12 here}

The coefficients in equation 3 are consistent with a physical understanding of cavitation in that:

1. As *C/H* ratio increases the fuel becomes more aromatic in nature and is more likely to react during bubble collapse to form carbon particles (c.f. the impact of aromatic content in diesel soot formation).
2. A flash point increase (and therefore vapour pressure decrease) results in more severe cavity collapse (higher T_{max}) producing higher levels of pyrolytic degradation and deposit formation.
3. As viscosity increases so does the cohesive forces between molecules, making it harder to form cavities. The reduction in the number of bubbles should result in less deposit formation.

355 **4.2 Mechanisms of particle growth**

356 The violent collapse of bubbles generates shear forces at the tip of the acoustic probe and
357 therefore promotes kinetically driven particle-particle collisions of the primary nanoparticles
358 that are formed during cavitation. This leads to aggregation and the formation of larger
359 particles with diameters in the micron range. Kinetically driven agglomeration rates are
360 defined by

$$J_{ok} = dN/dt = -2\alpha\gamma_s d^3 N^2/3 \quad (4)$$

361 where J_{ok} is the orthokinetic rate (m^{-3} s^{-1}) of change in primary particle number, N is the
362 primary particle number concentration (m^{-3}), γ_s is rate of shear (s^{-1}), d is the primary particle
363 diameter (m) and α is the collision efficiency (between 0 and 1).

364 If a constant rate of nanoparticle production from cavitation is assumed, it follows that

$$dN/dt = R_p - 2\alpha\gamma_s d^3 N^2/3 \quad (5)$$

365 where R_p is the rate of primary particle formation (m^{-3} s^{-1}) during sonication.

366 Equation 5 allows the primary particle number concentration to be defined as a function
367 of sonication time. A value for the rate of particle formation (R_p) (assuming γ_s = 1,000 s^{-1}, d
368 = 20 nm, ρ = 2,000 kg/m^3 and α = 1) can be set such that the predicted deposit mass (of
369 micron sized agglomerated material) matches that observed experimentally in the data from
370 Fig. 6. The results of this exercise are shown in Fig. 13 and reveals a good match between
371 measured and predicted deposit mass out to 120 minutes of sonication. An equilibrium
372 concentration of primary particles is established when

$$R_p = 2\alpha\gamma_s d^3 N_{eq}^2/3 \quad (6)$$

373 where N_{eq} is the equilibrated number concentration of primary particles (m^{-3}).

374 If the time required for this equilibrium (t_{eq}) to be established is short (~5 minutes) then
375 the mass of deposit essentially becomes proportional to the length of the ultrasound

376 treatment, as indeed is observed experimentally. The time required for the concentration of
377 primary particles to reach equilibrium (t_{eq}) is shortened if the size of the particles (d),
378 formation rate (R_p) or shear rate (γ_s) is increased. N_{eq} decreases if particle size (d) or shear
379 rate (γ_s) is reduced but increases with higher rates of formation (R_p). A reduction in collision
380 efficiency (α) will increase both t_{eq} and N_{eq}. From this exercise the primary particle number
381 concentration for sonicated 1-methylnaphthalene can be estimated to be in the region of 10^{12}
382 cm^{-3}.

383 {Fig. 13 here}

384 Once sonication is complete particle-particle collisions only occur as a consequence of
385 thermally induced motion. The Brownian movement of particles that gives rise to particle
386 agglomeration is described by

$$J_{pk} = dN/dt = -4\alpha kTN^2/3\eta \quad (7)$$

387 where J_{pk} is the perikinetic rate ($m^{-3}s^{-1}$) of change in primary particle number, N is the particle
388 number concentration (m^{-3}), k is Boltzmann's constant ($J\ K^{-1}$), T is temperature (K), α is the
389 collision efficiency (between 0 and 1) and η is the dynamic viscosity (Nsm^{-2}) of the liquid.
390 Integration of equation 7 gives

$$N = N_0 / (1+ 4\alpha kTN_0t/3\eta) \quad (8)$$

391 From which the half-life of the primary particles can be determined

$$t_{1/2} = 3\eta/4\alpha kTN_0 \quad (9)$$

392 Particle half-life is plotted as a function of particle number concentration in Fig. 14 based
393 upon a temperature of 300 K and a dynamic viscosity of $2x10^{-3}$ Nsm^{-2}. A high concentration
394 of primary particles (10^{12} cm^{-3}) will therefore undergo an initial rapid agglomeration to form
395 larger particles. However, further agglomeration of these larger particles will be slowed by
396 the drop in particle number and eventually the dispersion will become stable. It would
397 therefore appear that samples of diesel fuel sonicated for relatively short periods of time do

not contain sufficiently high numbers of primary particles for growth of secondary particles in the micron size range. However the contrasting behaviour of the sonicated 1-methylnaphthalene is consistent with a very high primary particle number concentration that is initially not detectable with the laser particle counter. During storage these nanoparticles grow into larger microparticles that fall within the detection limit of the technique and give rise to the sharp increase in the count of 1–2 μm particles.

{Fig. 14 here}

4.3 Implication for diesel fuel in modern common rail direct injection diesel engines

Fuel is known to undergo cavitation in injector nozzles, resulting in the formation of bubbles in regions where the liquid pressure falls below the fuel's vapour pressure [30-32]. This can occur at a pressure drop across an orifice or when fast moving flows turn sharp corners. If these bubbles return to high ambient pressure they collapse and produce areas of extreme temperature and pressure as a result of the adiabatic compression of the fuel vapour, in a manner analogous to that observed during acoustic cavitation.

Over the last six years there has been a growing awareness of field issues involving injector sticking in modern common rail compression ignition engines [33–36]. This is caused by the formation of internal diesel injector deposits (IDID), the occurrence of which has increased as fuel rail pressures (>2,000 bar) and injector nozzle temperatures (>200°C) have become higher [36,37]. These conditions result in stressed fuel, some of which is recycled back into the fuel tank rather than being burned.

Three main types of deposits have been identified, all of which are distinct from the coke-like material that forms in nozzle holes and which has historically been controlled through the use of detergent additives:

1. Soap deposits: Soft opaque material that is typically water soluble and comprised of metal (sodium, sometimes calcium) carboxylates or sodium chloride [35,38].
2. Lacquer deposits: Hard brown material that is insoluble in most solvents. Fourier transform infrared spectroscopy (FTIR) has identified the presence of amides (–C(O)NH–) leading to the origins of these deposits being linked to detergent molecules (in particular low molecule weight polyisobutylene succinimides, PIBSI) [33,35,39].
3. Carbonaceous deposits: Black material that has been observed on fuel filters and nozzle springs [40] as well as being linked to the reported phenomenon of black diesel fuel [41]. The origins of this material have proved to be somewhat difficult to identify, although there are reports of the material resembling combustion soot and being comprised of graphitic carbon [42–44].

A diesel vehicle (2008 registration plate) known to have an intermittent fault in which engine stalls occurred when it slowed to a standstill at junctions was sourced. The vehicle had been driven just over 100,000 miles on 191 tanks fills in a time period of three years. Examination of the vehicle revealed a fuel filter coated in black deposits and a visible suspension of fine material in samples of fuel taken from the tank – some of this material formed sediment when left to stand. TEM images show material that is similar to that generated by the ultrasound treatment of hydrocarbons, being comprised of small primary particles linked together into larger structures (Fig. 15). High magnification reveals the internal structure of these particles, within which can be seen layers of graphitic-like carbon (Fib 15b). The XRD spectrum of these deposits has a strong graphite peak at ~26.5° (Fig. 15c). The iron oxide-hydroxide (FeO(OH)), lepidocrocite was also found and is indicative of the presence of rust. Peaks consistent with calcium carbonate were cross matched with a small number of lozenge shaped particles seen in some of the TEM images. There are two

447 other peaks present which give a good fit to solid linear waxy saturated hydrocarbons (i.e.
448 $-(CH_2)_n-$).

449 {Fig. 15 here}

450 The phenomenon of cavitation in the high pressure fuel systems of modern common rail
451 diesel vehicles is therefore proposed as an explanation for the formation of deposits
452 comprising of fine particles. This material is observed to build up in the fuel over extended
453 periods of use. If large enough (>4 μm) it will be captured by the filter typically positioned
454 between the tank and the pump that delivers fuel into the high pressure rail that feeds each of
455 the injectors. Smaller sized material will however pass through this filter and be carried into
456 the injectors. If it migrates into regions within the injectors where there are low clearances
457 between moving surfaces (~1 μm) an impact upon injector response and function is possible.
458

459 **5. Conclusions**

460 Acoustically driven cavitation has been used to study the degradation chemistry that takes
461 place in hydrocarbons that fall within the middle distillate (C_8-C_{26}) range. The following
462 conclusions can be drawn from these experiments:

463 1. The high temperature produced by the implosion of bubbles that contain hydrocarbon
464 vapour and dissolved gases produces carbonaceous material (typical carbon levels of ca.
465 90 atomic % excluding H). These deposits form as dispersed micron sized particles that
466 are themselves comprised of agglomerated nanoparticles which have similarities to the
467 primary soot particles that are produced during the diffusion flame combustion of diesel
468 fuel. The carbon is a mixture of amorphous and graphitic material which also contains
469 significant quantities of oxygen (ca. 10 atomic % excluding H) in the form of hydroxyl,
470 carbonyl and ester or acid groups present on the particle surfaces.

2. The deposit-forming tendency of a hydrocarbon is strongly coupled to the number of unsaturated carbon-carbon bonds that are present or its C/H atomic ratio. The di-aromatic 1-methylnapthalene produces high levels of deposit during cavitation, whereas the paraffin hexadecane produces very few deposits.
3. The formation of the deposits can be reduced by increasing the flash point of the hydrocarbon. This increases the vapour pressure inside the bubbles and reduces the temperature (and pressure) that results from their implosion, slowing the reaction rates of the chemistry leading to particle formation. This reduction in deposit formation is most significant when the lower boiling hydrocarbon is paraffinic, as opposed to aromatic, in character.
4. During cavitation a mixture of primary nanoparticles and larger micron sized particles is produced. The dispersion of this material is stable if the particle number concentration of the primary particles is below a threshold value. However if high numbers of nanoparticles are present they can start to agglomerate to form additional numbers of micron sized particles during the storage of the sonicated liquid.
5. The chemistry and formation of deposits observed during the acoustic treatment of middle distillate hydrocarbons has been found to be similar to that seen during the hydrodynamic cavitation of fuel in modern common rail direct injection compression ignition engines. The material formed in these sonication experiments is compositionally similar to a suspension of particles sampled from fuel in the tank of a common rail diesel vehicle. The material is also consistent with the black deposits that are generally reported to build up on fuel filters and around the nozzle springs of injectors. Such material can affect the passage of fuel through the filter and possibly the correct function of the injectors.

Acknowledgements

The authors would like to acknowledge Dr. Chris Clayton for the initial proposal of using acoustic cavitation to study the degradation of middle distillate hydrocarbons and the contribution of Grant Middleton in the running of ultrasound experiments and the preparation of samples for analysis. The work has been financed by Shell Global Solutions.

References

[1] T. J. Mason and J. P. Lorimer, *Applied Sonochemistry: The Use of Power Ultrasound in Chemistry and Processing*, Weinham: Wiley-VCH, 2002.

[2] T. J. Mason, *Sonochemistry*, Oxford: Oxford University Press, 2005.

[3] K. S. Suslick and D. J. Flannigan, *Inside a Collapsing Bubble: Sonoluminescence and the Conditions during Cavitation*, Annu. Rev. Phys. Chem., 2008, **59**, 659–83.

[4] K. S. Suslick, D. A. Hammerton and R. E. Cline , *The Sonochemical Hot Spot*, J. Am. Chem. Soc., 1986, 108, 5641–2.

[5] E. B. Flint and K. S. Suslick, *The Temperature of Cavitation*, Science, 1991, **253**, 1397–9.

[6] Y. T. Didenko, W.B. McNamara and K. S. Suslick, *The Temperature of Multi-Bubble Sonoluminescence in Water*, J. Phys. Chem. A., J. Phys. Chem. A., 1999, **103**, 10783–88.

[7] W.B. McNamara, Y. T. Didenko and K. S. Suslick, *Sonoluminescence Temperatures During Multibubble Cavitation*, Nature, 1999, **401**, 772–5.

[8] L. Zechmeister and L. Wallcave, *On the Cleavage of Benzene, Thiophene and Furan Rings by Means of Ultrasonic Waves*, J. Am. Chem. Soc. 1955, **77**, 2853–55.

[9] L. Zechmeister and E. F. Magoon, *On the Ultrasonic Cleavage of the Pyridine Ring*, J. Am. Chem. Soc., 1956, **78**, 2149–50.

[10] D. L. Currell and L. Zechmeister, *On the Ultrasonic Cleavage of Some Aromatic and Heterocyclic Rings*, J. Am. Chem. Soc., 1958, **80**, 205–8.

[11] K. S. Suslick, J. J. Gawienowski, P. F. Schubert and H. H. Wang, *Alkane Sonochemistry*, J. Phys. Chem., 1983, 87, 2299–301.

[12] P. Riesz, D.Berdahl and C. L. Christman, *Free Radical Generation by Ultrasound in Aqueous and Nonaqueous Solutions*, Environmental Health Perspectives, 1985, **64**, 233–52.

[13] V. Misk and P. Riesz, *Free Radical Formation by Ultrasound in Organic Liquids: A Spin Trapping and EPR Study*, J. Phys. Chem., 1994, 98, 1634–40.

[14] V. Misk and P. Riesz, *EPR Study of Free Radicals Induced by Ultrasound in Organic Liquids II: Probing the Temperature of Cavitation Regions*, Ultrasonics Sonochemistry, 1996, **3**, 25–37.

[15] F. Cataldo, *Ultrasound-induced Cracking and Pyrolysis of Some Aromatic and Naphthenic Hydrocarbons*, Ultrasonics Sonochemistry, 2000, **7**, 35-43.

[16] R. Katoh, E. Yanase, H. Yokoi, S. Usuba, Y. Kakudate and S. Fujwara, *Possible New Route for the Production of C_{60} by Ultrasound*, Ultrasonics Sonochemistry, 1998, **5**, 37–8.

[17] R. Katoh, Y. Tasaka, E. Sekreta, M. Yumara, F. Ikazaki, Y. Kakudate and S. Fujiwara, *Sonochemical Production of a Carbon Nanotube*, Ultrasonics Sonochmeistry, 1999, **6**, 185–7.

[18] G. J. Price, *Recent developments in Sonochemical Polymerisation*, Ultrasonic Sonochemistry, 2003, **10**, 277–83.

[19] P. Kruus, D. McDonald and T. J. Patraboy, *Polymerisation of Styrene Initiated by Ultrasonics Cavitation*, J. Phys. Chem., 1987, **91**, 3041–7.

[20] P. Krus, M. O'Neil and D. Robertson, *Ultrasonic initiation of polymerisation*, Ultrasonics, 1990, **28**, 304–9.

[21] P. Krus and T. J. Patraboy, *Initiation of Polymerization with Ultrasound in Methyl Methacrylate*, J. Phys. Chem, 1985, **89**, 337984.

[22] R. Katoh, H. Yokoi, S. Usuba, Y. Kakudate and S. Fujiwara, *Sonochemical Polymerization of Benzene Derivatives: The Site of the Reaction*, Ultrasonics Sonochemistry, 1998, **5**, 69–72.

[23] G. J. Price and M. McCollom, *The Effect of High-Intensity Ultrasound on Diesel Fuels*, Ultrasonics Sonochemistry, 1995, **2**, S67–70.

[24] G. J. Price and M. McCollom, *Use of High-Intensity Ultrasound as a Potential Test Method for Diesel Fuel Stability*, Fuel, 1995, **74**, 1394-7.

[25] R. D. Lockett and M. Jeshani, *An Experimental Investigation into the Effect of Hydrodynamic Cavitation on Diesel*, Int. Journal of Engine Research, 2013, **6**, 606-21.

[26] G. C. Smith and P. J. Shuff, *Electron spectroscopy of carbonaceous materials*, Applied Surface Science, 1996, **103**, 199-203.

[27] B. E. Noltingk, E. A. Neppiras, *Cavitation Produced by Ultrasonics*, Proc. Phys. Soc. B, 1950 (London), **63B**, 674-85.

[28] E. A. Neppiras, *Acoustic Cavitation*, Phys. Rep. Rev. Sec. Phys. Lett., 1980, **61**,159–251.

[29] K. S. Suslick, J.J. Gawienowski, P.F. Schubert and H.H. Wang, *Sonochemistry in non-aqueous liquids*, Ultrasoncis, 1984, **22**, 33-6.

[30] H. Chaves, M. Knapp, A., Kubitzek and F. Obermeier, *Experimental Study of Cavitation in the Nozzle Hole of Diesel Injectors Using Transparent Nozzles*, SAE Paper 950290, 1995.

[31] C. Badock, R. Wirth, A. Fath and A. Leipertz, *Investigation of Cavitation in Real Size Diesel Injection Nozzles,* Int. J. Heat Fluid Flow, 1999;20(5):538–44.

[32] A. Andriotis, M. Gavaisesand C. Arcoumanis, *Vortex Flow and Cavitation in Diesel Injector Nozzles*, J. Fluid Mech. 2008; 610:195–215.

[33] J. Ullmann, M. Gedulig, H. Stutzenberger, R. Caprotti and G. Balfour, *Investigation into the Formation and Prevention of Internal Diesel Injector Deposits,* SAE Paper 2008-01-0926, 2008.

[34] S. Cook and P. Richards, *Possible Influence of High Injection Pressure on Diesel Fuel Stability: A Review and Preliminary Study*, SAE Paper 2009-01-1878, 2009.

[35] P. Lacey, S. Gail, J.M. Kientz, N. Milovanovic and C. Gris, *Internal Fuel Injector Deposits*, SAE Paper 2011-01-1925, 2011.

[36] T. Omori, A. Tanaka, K. Yamada and S. Bunne, *Biodiesel Deposit Formation Mechanism and Improvement of Fuel Injector Equipment (FIE),* SAE Paper 2011-01-1935.

[37] A. Theodorakakos, N. Mitroglou and M. Gavaises, *Simulation of Heating Effects in Cavitating Flows Through Diesel Fuel Injectors Caused by Extreme Fuel Pressurisation,* 8th Int. Symp. on Cavitation, 14-16 August, 2012.

[38] M. Arondel, H. Rodeschini and M. Lopes and B. Dequenne, *Fuel Additives for Reduction of Internal Diesel Injector Deposits (IDID, "lacquering"): A Critical and Priority Route*, SAE Paper No. 2012-01-1687, 2012.

[39] X. Fang and J. M. Galante-Fox, *Diesel Fuel Additive*, US Patent Application No. US 2011/0302828 A1, 2011

[40] P. Lacey, S. Gail and C. Daveau, *Internal Injector Deposit Overview*, SAE Injector Deposits Workshop, 18th September 2012.

[41] S. R. Westbrook, *Analysis of Some Unusual Diesel Fuel Contaminants*, 9th Int. Filtration Conference, Paper No. IFC09-015, July 9, 2009.

[42] J. Baker, P. Richards, M. Goodwin and J. Wooler, *Influence of High Pressure on Diesel Fuel Stability: A Study of Resultant Deposits, SAE Paper 2009-01-1877, 2009.*

[43] J. Baker, P. Richards, C. Snape and W. Meredith, *A Novel Technique for Investigating the Nature and Origins of Deposits Formed in High Pressure Fuel Injection Equipment*, SAE Paper 2009-01-2637, 2009.

[44] J. Baker, P. Richards, C. Snape and W. Meredith, *Diesel Injector Deposits – An Issue That Has Evolved with Engine Technology*, SAE Paper 2011-01-1923, 2011.

602 **Figure Captions**

603 Colour figures in electronic versions only.

604

605 **Fig. 1.** Schematic of the experimental apparatus used for the sonication of hydrocarbon

606 liquids.

607 **Fig. 2.** 1-Methylnaphthalene (50 mL) before (a) and after (b) 20 kHz ultrasound treatment (6

608 kJ mL^{-1}) for 1 h. An addition of 50 mL of *n*-heptane was made before centrifuging the

609 suspension (4,000 r min^{-1} for 20 minutes) and filtration through a 0.7 μm microfiber paper

610 (c).

611 **Fig. 3.** TEM images (a, b and c) and XRD pattern (d) of particles formed in sonicated 1-

612 methylnaphthalene.

613 **Fig. 4.** Carbon 1s XPS (a) and the X-ray excited carbon KVV Auger spectra (b) of four

614 samples (S1-4) of particles all produced by the sonication of 1-methylnaphthalene.

615 **Fig. 5.** TEM images of particles formed in 1-methylnaphthalene when ultrasound is

616 delivered indirectly using a cup-horn. The low (a) and high (b) magnification images show

617 similar features to those presented in Fig. 3.

618 **Fig. 6.** Relationship between deposit mass and the sonication time (6 kJ mL^{-1} h^{-1}) of 50 mL

619 of 1-methylnaphthalene.

620 **Fig. 7.** Deposit mass produced by the 1 h sonication (6 kJ mL^{-1}) of 50 mL volumes of 1-

621 methylnaphthalene and mixtures of 1-methylnaphthalene with 20% v/v of hexadecane,

622 decalin or tetralin as a function of C/H atomic ratio. The bars show the typical C/H range for

623 the different generic classes of hydrocarbons present in diesel fuel. (TriAr – tri-aromatics,

624 NdiAR – naphthenic-di-aromatics, DiAr – di-aromatics, NmoAr – naphthenic mono-

625 aromatics, MoAr – mono-aromatics, DiN – di-naphthenics, N- naphthenics, P- paraffins).

Fig. 8. The change in deposit mass produced by blending 1-3% (v/v) of a second hydrocarbon into 1-methylnaphthalene and treating with ultrasound (6 kJ mL^{-1} h^{-1}). Repeat measurements of the deposit mass produced from just 1-methylnaphthalene had a relative standard deviation of 2.8% (n=10).

Fig. 9. Total particle number concentration in diesel fuel and 1-methylnaphthalene (50 mL) after 0–80 minutes sonication (6 kJ mL^{-1} h^{-1}).

Fig. 10. Particle number concentration as a function of particle diameter in diesel fuel and 1-methylnaphthalene (50 mL) after 0–80 minutes sonication (6 kJ mL^{-1} h^{-1}).

Fig. 11. Change in particle number concentration with storage time for diesel fuel and 1-methylnaphthalene after sonication (6 kJ mL^{-1} h^{-1}).

Fig. 12. The correlation between measured and empirically predicted deposit mass.

Fig. 13. Deposit formation in 1-methylnapthalene and the predicted equilibrated concentration of primary particles (γ_s = 1,000 s^{-1}, d = 20 nm, ρ = 2,000 kg/m^3 and α = 1).

Fig. 14. Relationship between half-life and primary particle number concentration (T = 300 K and η = 2x10^{-3} N s m^{-2}).

Fig. 15. TEM images (a and b) and XRD pattern (c) of particles taken from the fuel tank of a diesel vehicle.

Table titles

Table 1. Number concentration (cm^{-3}) and mean diameter (μm) (in italics) of particles produced by the cavitation (6 kJ mL^{-1} h^{-1}) of diesel fuel and 1-methylnaphthalene (1-MN) followed by storage.

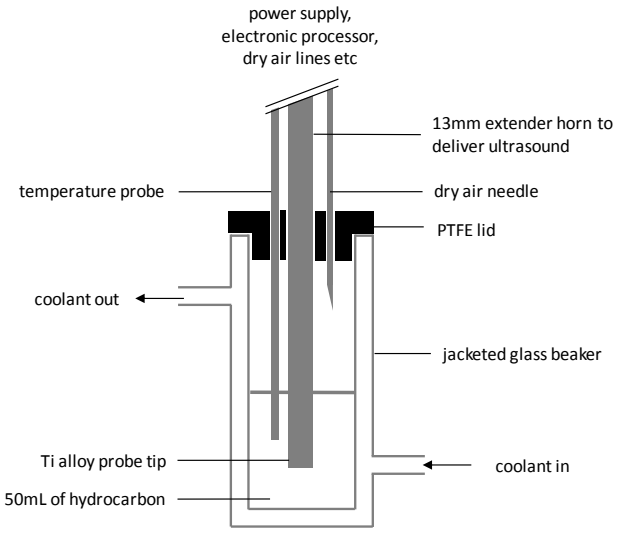

649

650 **Fig. 1.** Schematic of the experimental apparatus used for the sonication of hydrocarbon

651 liquids.

652

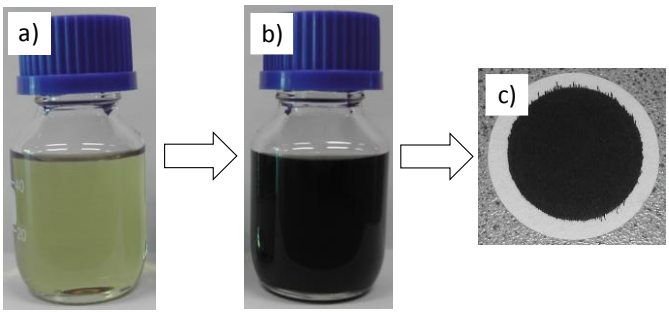

Fig. 2. 1-Methylnaphthalene (50 mL) before (a) and after (b) 20 kHz ultrasound treatment (6 kJ mL^{-1}) for 1 h. An addition of 50 mL of *n*-heptane was made before centrifuging the suspension (4,000 r min^{-1} for 20 minutes) and filtration through a 0.7 µm microfiber paper (c).

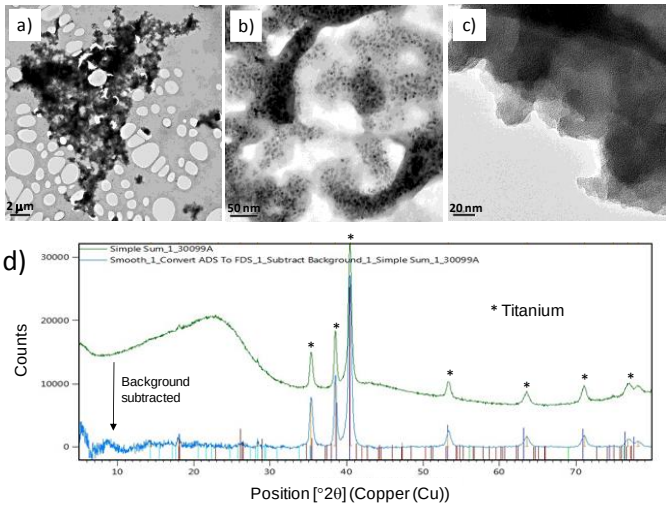

658

659 **Fig. 3.** TEM images (a, b and c) and XRD pattern (d) of particles formed in sonicated 1-

660 methylnaphthalene.

661

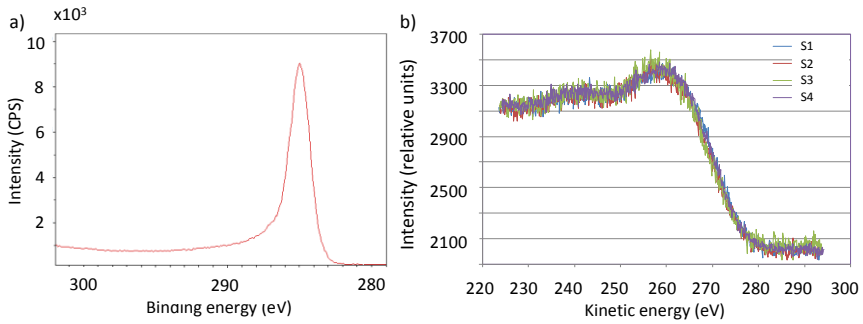

662

663 **Fig 4.** Carbon 1s XPS (a) and the X-ray excited carbon KVV Auger spectra (b) of four

664 samples (S1-4) of particles all produced by the sonication of 1-methylnaphthalene.

665

666 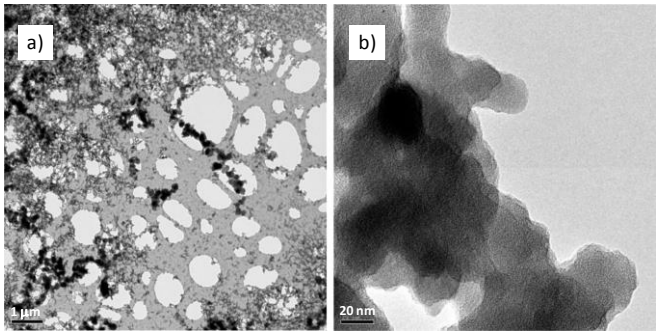

667 **Fig. 5.** TEM images of particles formed in 1-methylnaphthalene when ultrasound is
668 delivered indirectly using a cup-horn. The low (a) and high (b) magnification images show
669 similar features to those presented in Fig. 3.

670

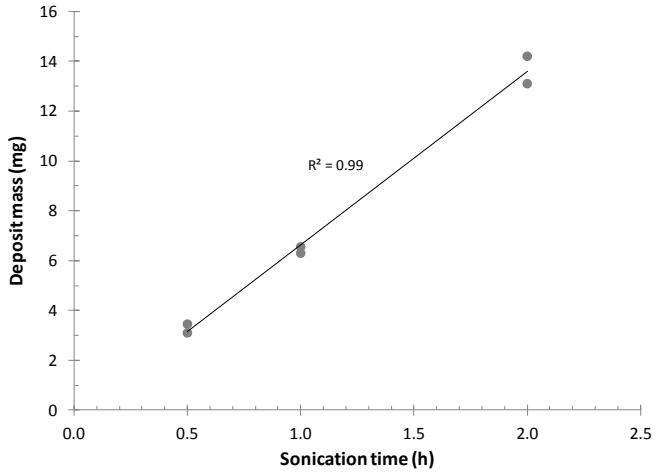

671

672 **Fig. 6.** Relationship between deposit mass and the sonication time (6 kJ mL^{-1} h^{-1}) of 50 mL

673 of 1-methylnaphthalene.

674

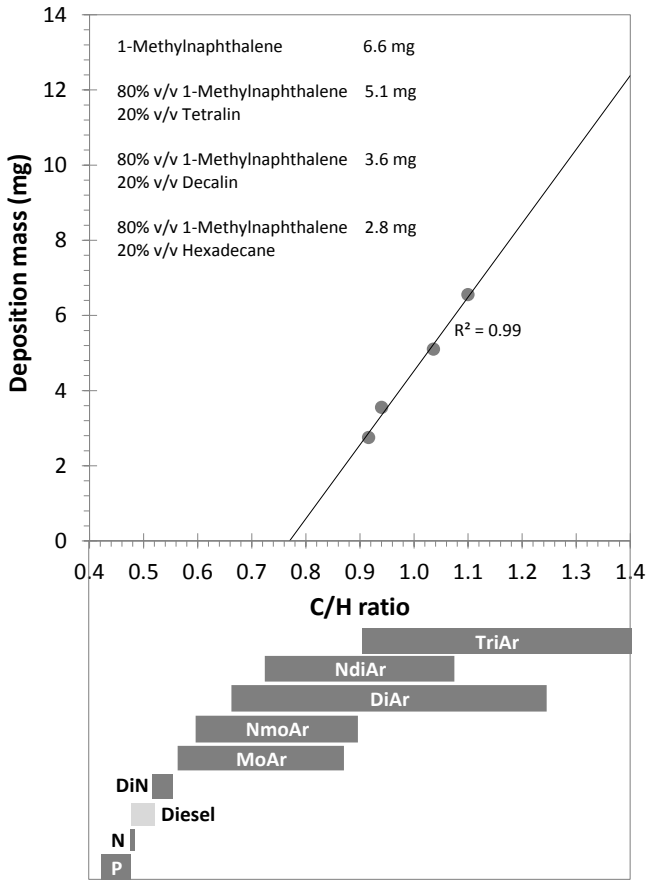

675

676 **Fig. 7.** Deposit mass produced by the 1 h sonication (6 kJ mL^{-1}) of 50 mL volumes of 1-
677 methylnaphthalene and mixtures of 1-methylnaphthalene with 20% v/v of hexadecane,
678 decalin or tetralin as a function of C/H atomic ratio. The bars show the typical C/H range for
679 the different generic classes of hydrocarbons present in diesel fuel. (TriAr – tri-aromatics,
680 NdiAR – naphthenic-di-aromatics, DiAr – di-aromatics, NmoAr – naphthenic mono-
681 aromatics, MoAr – mono-aromatics, DiN – di-naphthenics, N- naphthenics, P- paraffins).

682

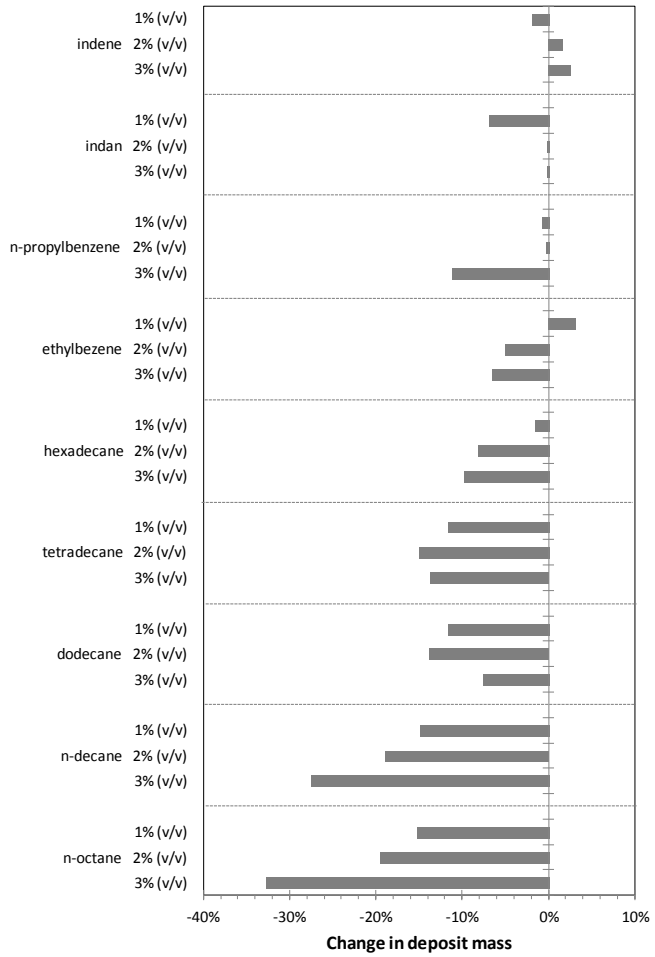

683

684 **Fig. 8.** The change in deposit mass produced by blending 1-3% (v/v) of a second

685 hydrocarbon into 1-methylnaphthalene and treating with ultrasound (6 kJ mL^{-1} h^{-1}). Repeat

686 measurements of the deposit mass produced from just 1-methylnaphthalene had a relative

687 standard deviation of 2.8% (n=10).

688

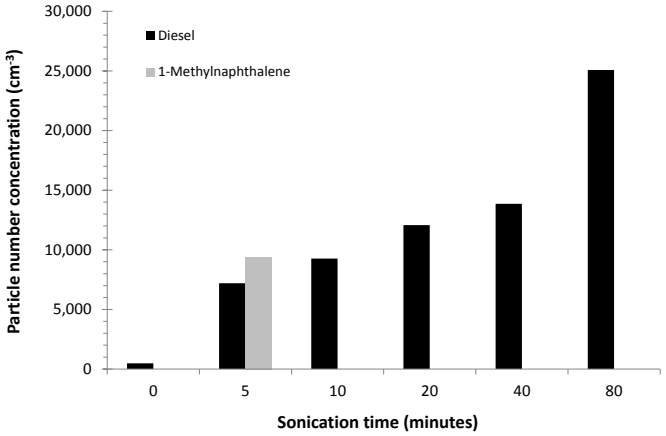

689

690 **Fig. 9.** Total particle number concentration in diesel fuel and 1-methylnaphthalene (50 mL)

691 after 0–80 minutes sonication (6 kJ mL^{-1} h^{-1}).

692

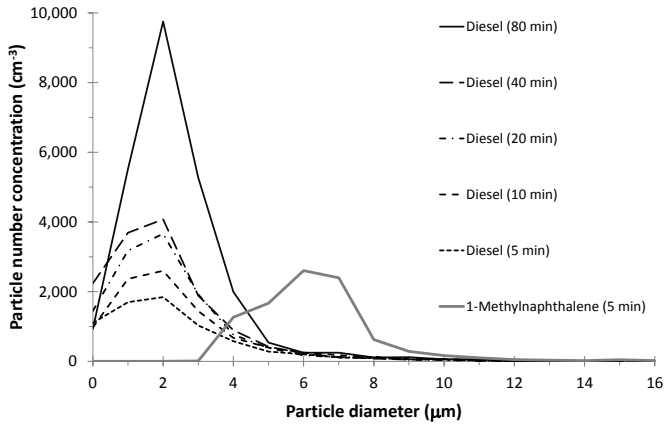

693

694 **Fig. 10.** Particle number concentration as a function of particle diameter in diesel fuel and 1-

695 methylnaphthalene (50 mL) after 0–80 minutes sonication (6 kJ mL^{-1} h^{-1}).

696

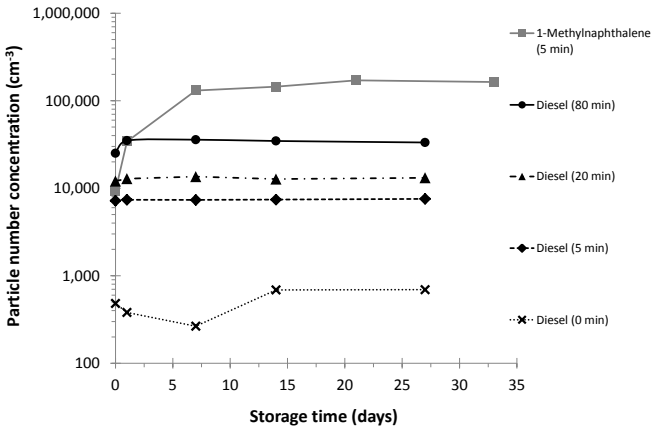

697

698 **Fig. 11.** Change in particle number concentration with storage time for diesel fuel and 1-

699 methylnaphthalene after sonication (6 kJ mL^{-1} h^{-1}).

700

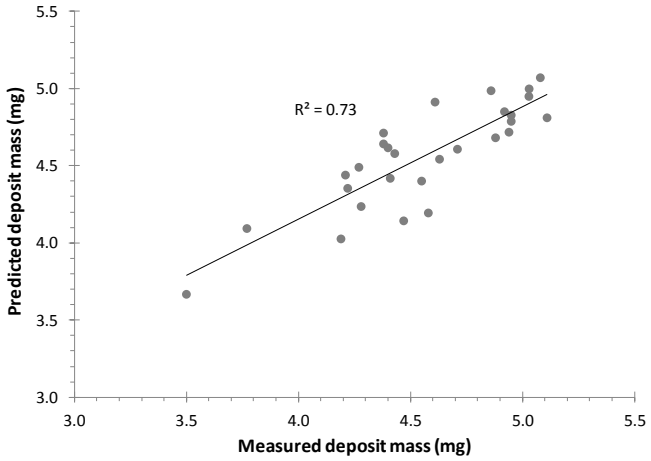

Fig. 12. The correlation between measured and empirically predicted deposit mass.

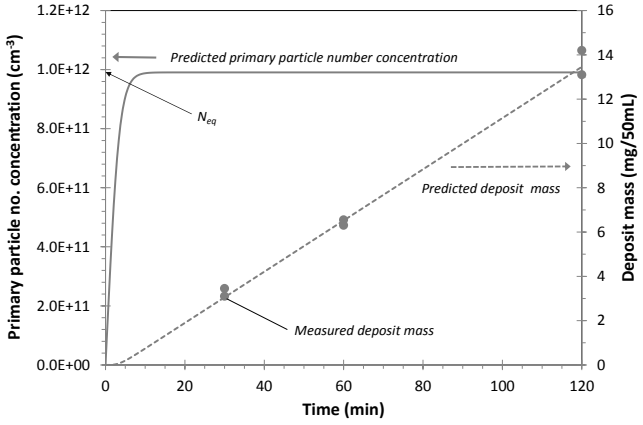

704

705 **Fig. 13.** Deposit formation in 1-methylnapthalene and the predicted equilibrated

706 concentration of primary particles (γ_s = 1,000 s^{-1}, d = 20 nm, ρ = 2,000 kg/m^3 and α = 1).

707

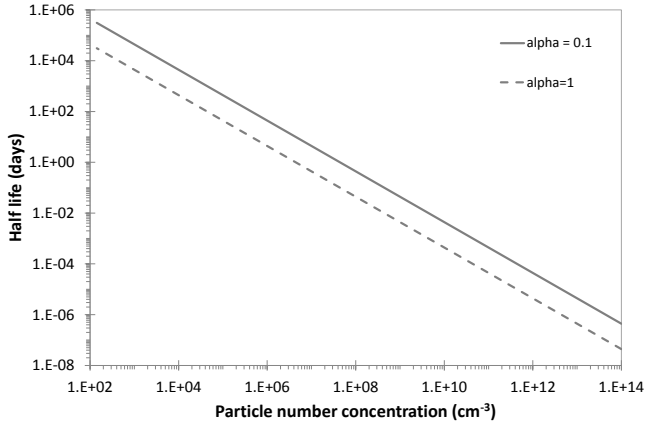

708

709 **Fig. 14.** Relationship between half-life and primary particle number concentration (T = 300

710 K and η = 2x10^{-3} N s m^{-2}).

711

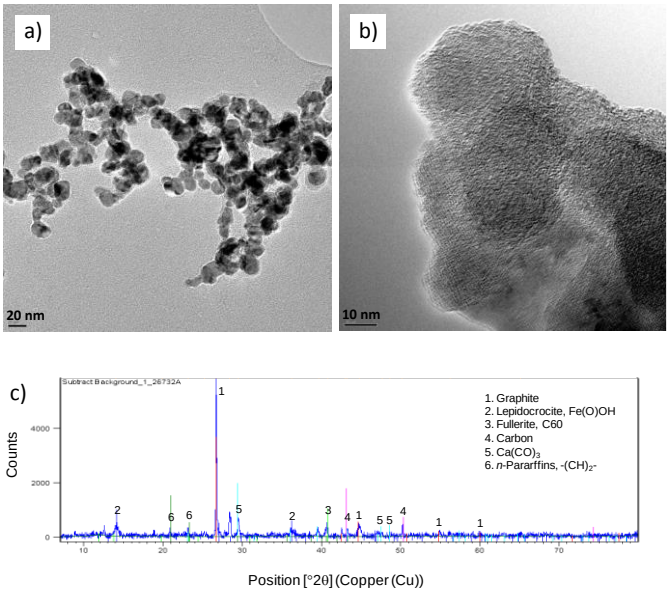

712

713 **Fig. 15.** TEM images (a and b) and XRD pattern (c) of particles taken from the fuel tank of a

714 diesel vehicle.

715

Table 1. Number concentration (cm^{-3}) and mean diameter (μm) (in italics) of particles produced by the cavitation (6 kJ mL^{-1} h^{-1}) of diesel fuel and 1-methylnaphthalene (1-MN) followed by storage.

Storage time (days)	**Diesel cavitation time** (min)						**1-MN cavitation time** (min)
	0	**5**	**10**	**20**	**40**	**80**	**5**
0	482 *2.3*	7,196 *2.7*	9,271 *2.7*	12,070 *2.5*	13,856 *2.1*	25,086 *2.6*	9,397 *6.6*
1	381 *1.6*	7,388 *2.7*	11,030 *3.6*	12,848 *2.1*	15,909 *2.7*	35,021 *3.0*	34,160 *5.0*
7	265 *4.2*	7,354 *2.6*	10,799 *2.7*	13,576 *2.5*	16,378 *2.2*	35,868 *3.6*	134,745 *1.8*
14	689 *4.1*	7,413 *3.0*	10,711 *3.0*	12,733 *2.3*	15,267 *2.0*	34,671 *3.6*	144,878 *2.3*
21	– –	– –	– –	– –	– –	– –	170,955 *1.6*
27	694 *3.8*	7,556 *2.6*	11,477 *2.8*	13,158 *2.3*	16,225 *2.4*	33,341 *2.9*	– –
33	– –	– –	– –	– –	– –	– –	163,468 *1.9*